

# EIGHT YEARS OF SOHO: SOME HIGHLIGHTS

B. FLECK

*ESA Research and Scientific Support Department*

*c/o NASA/GSFC, Mailcode 682.3, Greenbelt, MD 20771, USA*

**Abstract.** Since its launch on 2 December 1995, the joint ESA/NASA SOHO mission has provided a wealth of information about the Sun, from its interior, through the hot and dynamic atmosphere, to the solar wind and its interaction with the interstellar medium. Analysis of the helioseismology data from SOHO has provided the first images of structures and flows below the Sun's surface and has shed new light on a number of structural and dynamic phenomena in the solar interior, such as the absence of differential rotation in the radiative zone, subsurface zonal and meridional flows, and sub-convection-zone mixing. Evidence for an upward transfer of magnetic energy from the Sun's surface toward the corona has been established. The ultraviolet imagers and spectrometers have revealed an extremely dynamic solar atmosphere where plasma flows play an important role. Electrons in coronal holes were found to be relatively "cool", whereas heavy ions are extremely hot and have highly anisotropic velocity distributions. The source regions for the high speed solar wind have been identified and the acceleration profiles of both the slow and fast solar wind have been measured. SOHO has also revolutionized our space weather forecasting capabilities by providing a continuous stream of images of the dynamic atmosphere, extended corona, and activity on the far side of the Sun. At the same time, SOHO's easily accessible images and movies have captured the imagination of the science community and the general public alike. This article summarizes some of the key findings from 8 years of SOHO.

## 1. Introduction

The Solar and Heliospheric Observatory (SOHO) is a project of international cooperation between ESA and NASA to study the Sun, from its deep core to the outer corona, and the solar wind (Domingo *et al.*, 1995). It carries a complement of twelve sophisticated instruments, developed and furnished by twelve international PI consortia involving 39 institutes from fifteen countries (Belgium, Denmark, Finland, France, Germany, Ireland, Italy, Japan, Netherlands, Norway, Russia, Spain, Switzerland, United Kingdom, and the United States). Detailed descriptions of all the twelve instruments on board SOHO as well as a description of the SOHO ground system, science operations and data products together with a mission overview can be found in Fleck *et al.* (1995).

### 1.1. MISSION STATUS

SOHO was launched by an Atlas II-AS from Cape Canaveral Air Station on 2 December 1995, and was inserted into its halo orbit around the L1 Lagrangian point on 14 February 1996. The launch was so accurate and the orbital maneuvers were so efficient that enough fuel remains on board to maintain the halo orbit for several decades, many times the lifetime originally foreseen (up to six years). An extension of the SOHO mission for a period of five years beyond its nominal lifetime, i.e. until March 2003, was approved by ESA's Science Programme Committee in 1997, and a further extension until March 2007 was approved in February 2002.

An unexpected loss of contact occurred on 25 June 1998. Fortunately, the mission could be completely recovered in one of the most dramatic rescue efforts in space, and normal operations could be resumed in mid-November after the successful recommissioning of the spacecraft and all twelve instruments. When the last on-board gyro failed on 21 December 1998, SOHO went into Emergency Sun Reacquisition (ESR) mode. In a race against time — the ESR thruster firings consumed an average of about 7 kg of hydrazine per week - engineers at ESTEC and Matra Marconi Space developed software to exit ESR mode without a gyro and allow gyroless operation of the spacecraft. The first gyroless reaction wheel management and station keeping manoeuvre was performed on 1 February 1999, making SOHO the first three-axis-stabilised spacecraft to be operated without a gyro. A new Coarse Roll Pointing (CRP) mode, which uses the reaction wheel speed measurements to monitor and compensate for roll rate changes, was successfully commissioned in September 1999. The CRP mode is almost two orders of magnitude more stable than using gyros. It also acts as an additional safety net between the normal mode and ESR mode, making SOHO perhaps more robust than ever.

In early May 2003, the East-West pointing mechanism of SOHO's High Gain Antenna (HGA) started missing steps; by late June it appeared stuck. Using both primary and redundant motor windings simultaneously, the mechanism was parked in a position that maximises the time it can be used throughout a 6-month halo orbit, with the spacecraft rotated by 180 degrees for half of each orbit and with "keyhole periods" twice per orbit. During the keyholes the Low Gain Antenna can be used with larger DSN stations to receive science telemetry, but data losses of varying magnitude occur depending on the competition for these resources.

### 1.2. OPERATIONS

The SOHO Experimenters' Operations Facility (EOF), located at NASA's Goddard Space Flight Center (GSFC), serves as the focal point for mission

science planning and instrument operations. At the EOF, the experiment teams receive real-time and playback telemetry, process these data to determine instrument commands, and send commands directly from their workstations through the ground system to their instruments, both in near real-time and on a delayed execution basis.

From the very beginning of the mission, much of the observing time of the SOHO experiments has been devoted to coordinated campaigns. As of mid-February 2004, the SOHO campaign database lists a total of 955 coordinated campaigns. Of these, 315 involved ground-based observatories, 110 involved Yohkoh, and 365 involved TRACE.

With over 1500 articles in the refereed literature and even more articles in conference proceedings and other publications, it is impossible to cover adequately all the exciting work that has been done in the past eight years. Instead, we can only touch upon some selected results.

## 2. Irradiance Variations

The total solar irradiance (TSI) is measured by the VIRGO experiment with two types of radiometers, PMO6V and DIARAD, allowing a first independent and internally consistent determination of possible long-term changes. By comparing the VIRGO measurements with ACRIM-II on UARS, Fröhlich (2002) estimates the uncertainty of the long-term precision over the first 7 years of the SOHO mission to less than  $\pm 15$  ppm, or about 2 ppm/yr.

Fröhlich & Lean (2002) compiled the composite TSI from 1978 through 2002 with an overall precision of order  $0.05 \text{ Wm}^{-2}$  and a secular trend uncertainty of  $\pm 3$  ppm/year (Fig. 1). They did not find any significant trend of TSI over the past 24 years. Willson and Mordvinov (2003), who neglect the corrections of the NIMBUS-7 HF instrument data set during the period of the gap between ACRIM-I and II, disagree. They instead claim a secular increase of TSI of about the amount of the HF correction. Interpretation of the TSI record, whether as a steady cycle with no underlying secular change or as showing an increasing trend, has broad social and political impacts as governments make decisions on their responses (if any) to global warming.

In recent years there has been significant effort in modeling the TSI variations by several groups (see e.g. Krivova *et al.*, 2003, and references therein). Their models reconstruct irradiance variations from model atmospheres for the quiet Sun, sunspot umbra and penumbra, and faculae, with a contrast depending on the magnetic field strength. The areas of faculae and network are determined empirically from MDI magnetograms, and the areas of sunspot umbrae and penumbrae from MDI intensity images. While some would argue that such a “superficialist” interpretation of the origin of

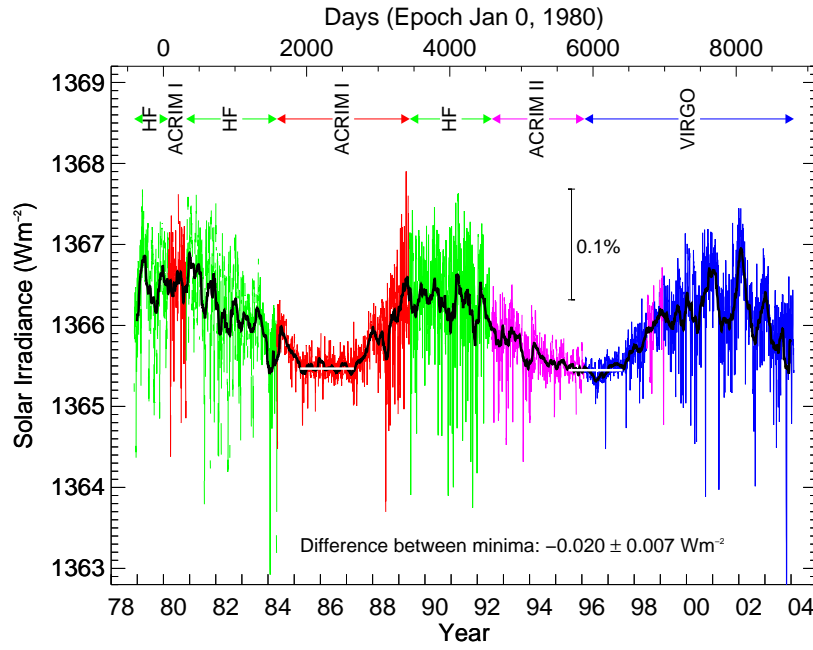


Figure 1. The composite TSI from 1978 through early 2004. Courtesy C. Fröhlich/VIRGO.

irradiance variations ignores potentially important subsurface physics, the agreement of model and observations in Fig. 2 is remarkable.

### 3. Solar Interior Dynamics and Flows

#### 3.1. SOLAR MODELS AND NEUTRINO FLUX

For many decades the solar neutrino puzzle has been one of the most fundamental unsolved problems in astrophysics (e.g. Bahcall & Ostriker, 1997). Helioseismology, by putting ever more stringent constraints on the neutrino flux emitted by nuclear reactions in the core (e.g. Turck-Chièze *et al.*, 2001), has played a key role in solving this puzzle. Turck-Chièze *et al.* (2001) have used sound speed and density profiles inferred from GOLF and MDI data to construct a spherically symmetric seismically adjusted model. Critically important in that work was the prior identification of low-order low degree modes ( $n < 9$ ,  $l = 0, 1, 2$ ), which are relatively insensitive to the uncertain structure and dynamics of the turbulent surface layers of the Sun. They determined the emitted neutrino flux of their seismic model and demonstrated that it is unlikely that the deficit of the neutrino flux measured on Earth can be explained by a spherically symmetric classical model

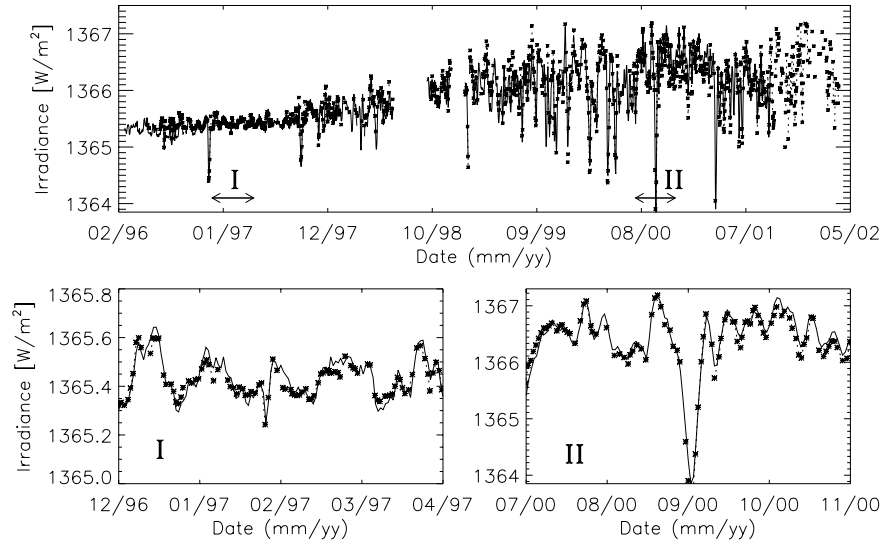


*Figure 2.* Top panel: Reconstruction (asterisks connected by dotted curve when there are no data gaps) of total solar irradiance for about 1500 individual days between 1996 and 2002, i.e. from the minimum of cycle 23 to its maximum. The irradiance record measured by VIRGO is represented by the solid line. The bottom panels show a zoom-in to two shorter intervals at different activity levels labeled a and b in the top panel. The agreement between measurements and reconstructions is remarkable. From Krivova *et al.* (2003).

without neutrino flavor transitions. The neutrino problem was eventually put to rest by the Sudbury Neutrino Observatory (SNO) measurements, which provided strong evidence for solar  $\nu_e$  flavor transformation (Ahmad *et al.*, 2002).

### 3.2. STILL NO G-MODES

Gabriel *et al.* (2002) performed a critical statistical analysis of over five years of GOLF data and found no statistically significant evidence for g-mode oscillations in the observed range of 150–400  $\mu\text{Hz}$ . They could set a new upper limit for the velocity amplitudes at the solar surface of 6 mm/s. The previous upper limit based on work by the Phoebus group (Appourchaux *et al.*, 2000) was 10 mm/s. Gabriel *et al.* found three possible peaks at 209.974  $\mu\text{Hz}$ , 218.374  $\mu\text{Hz}$ , and 284.666  $\mu\text{Hz}$ , with the last one tentatively identified as one member of the  $m = \pm 1$  multiplet of the  $n = 1$ ,  $l = 1$  p-mode. The statistical significance of the other two peaks, previously tentatively identified as possible g-mode candidates from GOLF data, is shown

to be insufficient, within the present assumptions regarding the nature of the signal.

### 3.3. CORE ROTATION

Couvidat *et al.* (2003) derived the radial rotation profile of the deep interior of the Sun from the analysis of low-order GOLF and MDI sectoral modes ( $l \leq 3$ ,  $6 \leq n \leq 15$ ,  $|m| = l$ ) and LOWL data ( $l > 3$ ). After removing the effects of the latitudinal variation of the rotation in the convection zone, they obtain a flat rotation profile down to  $0.2 R_{\odot}$ . This puts strong constraints on the redistribution of angular momentum. Without the correction of the splittings to account for the differential rotation in the convection zone, the inferred rotation rate near the core shows a decrease.

### 3.4. CONVECTION ZONE ROTATION

The nearly uninterrupted MDI data yield oscillation power spectra with an unprecedented signal-to-noise ratio that allow the determination of the frequency splittings of the global resonant acoustic modes of the Sun with exceptional accuracy. The inversions of these data have confirmed that the decrease of the angular velocity  $\Omega$  with latitude seen at the surface extends with little radial variation through much of the convection zone, at the base of which is an adjustment layer, called the “tachocline”, leading to nearly uniform rotation deeper in the radiative interior (Schou *et al.*, 1998). Further a prominent rotational shearing layer in which  $\Omega$  increases just below the surface is discernible at low to mid latitudes. Schou *et al.* (1998) have also been able to study the solar rotation closer to the poles than has been achieved in previous investigations. The data have revealed that the angular velocity is distinctly lower at high latitudes than the values previously extrapolated from measurements at lower latitudes based on surface Doppler observations and helioseismology.

### 3.5. TACHOCLINE OSCILLATIONS

Using data from MDI and the GONG network, Howe *et al.* (2000b) detected changes in the rotation of the Sun near the base of the convection zone, with unexpected periods of  $\approx 1.3$  year near the equator, possibly faster ( $\approx 1$  year) at high latitudes. Inversion of the global-mode frequency splittings revealed temporal changes in the angular velocity  $\Omega$  of up to 6 nHz above and below the tachocline, with the peak amplitude at  $0.72 R_{\odot}$  and an anticorrelated variation at  $0.63 R_{\odot}$ . The changes are most pronounced near the equator and at high latitudes and are a substantial fraction of the average 30 nHz

difference in  $\Omega$  with radius across the tachocline at the equator. The 1.3-year periodicity is in stark contrast to the 11-year period of the sunspot cycle. More recent work by Howe (2003) indicates that the amplitude of the 1.3-year variations of the rotation rate near the tachocline has been greatly reduced in recent years. It is interesting to note that this reduction coincided with higher solar activity, and it will be interesting to see whether this periodicity will show up again during the decreasing part of the solar cycle.

### 3.6. ZONAL FLOWS

From f-mode frequency splittings of MDI data, Kosovichev and Schou (1997) detected zonal variations of the Sun's differential rotation, superposed on the relatively smooth latitudinal variation in  $\Omega$ . These alternating zonal bands of slightly faster and slower rotation show velocity variations of about  $\pm 5$  m/s at a depth of 2–9 Mm beneath the surface and extend some 10 to 15° in latitude. They appear to coincide with the evolving pattern of “torsional oscillations” reported from earlier surface Doppler studies. Later studies (e.g. Howe *et al.*, 2000a) showed that these relatively weak flows are not merely a near-surface phenomenon, but extend downward at least 60 Mm (some 8% of the solar radius), and thus are evident over a significant fraction of the nearly 200 Mm depth of the solar convection zone. Indeed, Vorontsov *et al.* (2002), by applying a novel inversion method to the MDI rotational splitting data of 1996–2002, found evidence that these zonal shear flows (or “torsional oscillations”) can penetrate to the bottom of the convection zone. It appears that the entire solar convective envelope is involved in the torsional oscillations, with phase propagating poleward and equatorward from midlatitudes at all depths. This challenges the previous models of torsional oscillations as a secondary effect of migrating sunspot zones.

### 3.7. MERIDIONAL FLOWS

Meridional flows from the equator to the poles have been observed before on the solar surface in direct Doppler shift measurements (e.g. Duvall, 1979). The time-distance measurements by Giles *et al.* (1997) provided the first evidence that such flows persist to great depths, and therefore may play an important role in the 11-year solar cycle. They found the meridional flow to persist to a depth of at least 26 Mm, with a depth averaged velocity of  $23.5 \pm 0.6$  m/s at mid-latitude. Since then several methods of local helioseismology have been used to measure the meridional flows in the upper convection zone and their changes with the solar cycle (e.g. Beck *et al.*, 2002, Haber *et al.*, 2002). These flows play a key role in flux-transport dynamo

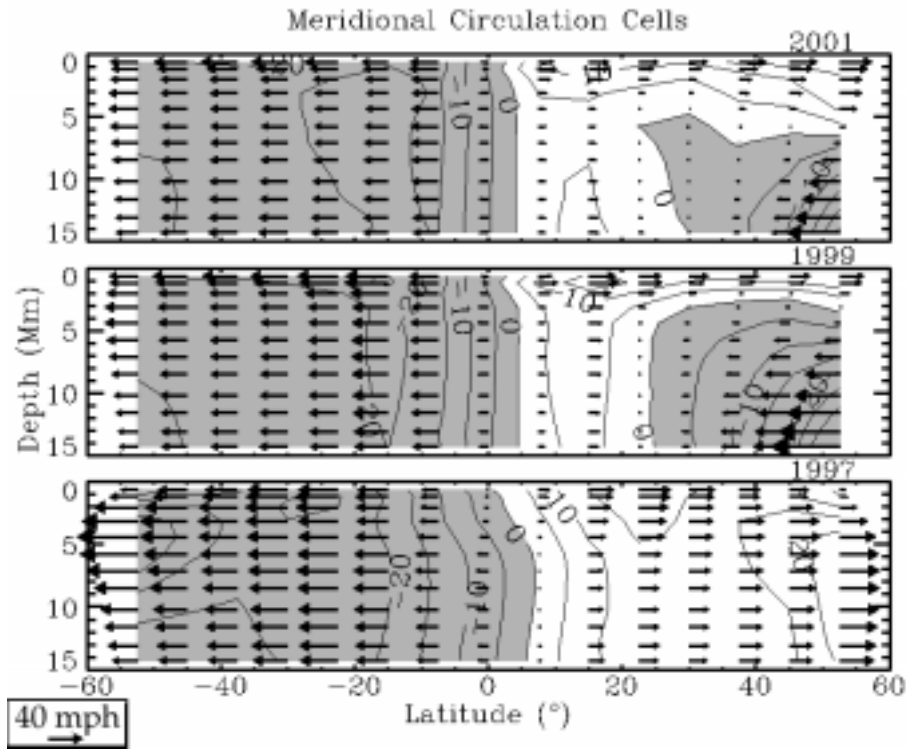


*Figure 3.* Meridional flow averaged in time and longitude, shown as a function of latitude and depth during the rising phase of cycle 23 (years 1997, 1999, and 2001). Underlying the vector fields are contours of constant meridional flow, with contours labeled in m/s. Regions of southerly flow are indicated by negative contours and are shaded gray. Starting in 1998, an additional circulation cell appears in the northern hemisphere (positive latitudes). This cell manifests as a submerged region of equatorward flow lying below poleward flow at the surface and appearing as the gray zon within the northern hemisphere. The breaking of symmetry between the southern hemisphere, which has a fairly uniform flow, and the northern hemisphere, which has varying multiple cells, is quite striking. Courtesy of D. Haber.

models of the cycle, by transporting the magnetic flux to the polar regions and causing the polarity reversals. The common result is that the meridional circulation slows down when the activity level is higher because of the additional flows converging around active regions in the activity belts. In addition, Haber *et al.* (2002) have studied how meridional circulation varies with depth over time, and found surprising evidence of the appearance and evolution of a submerged meridional cell during the years 1998-2001, which arose in the northern hemisphere and disrupted the orderly poleward flow and symmetry about the equator that is typically observed (Fig. 3).



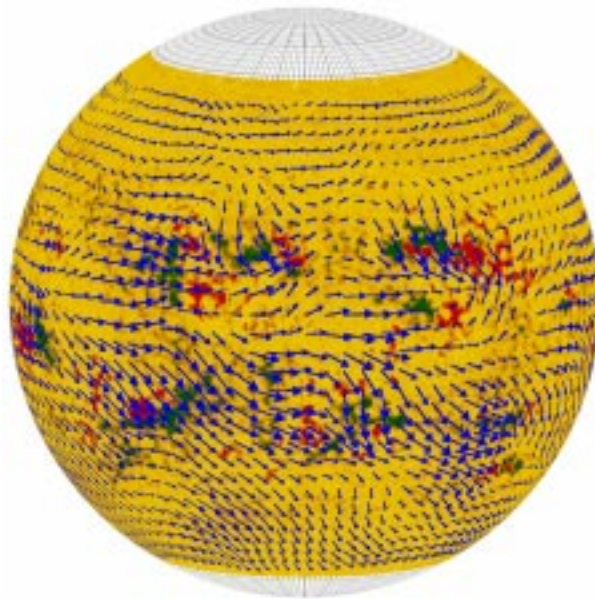


*Figure 4.* Large-scale flows in the upper convection zone obtained by ring-diagram analysis of 28 days of MDI Dynamics data from April 2002, superposed on an MDI magnetogram. Courtesy of D. Haber.

### 3.8. SOLAR SUBSURFACE WEATHER

The “ring diagram” analysis of MDI Dynamics data by Haber *et al.* (2002) has also revealed persistent patterns of large-scale flows in the upper convection zone (Fig. 4). These results led to a new concept of “Solar Subsurface Weather” connecting the effects of the synoptic flows to the development of solar activity. The initial results are promising, and may result in a new approach to long-term space weather forecasting, based on the dynamics of the upper convection zone.

### 3.9. FAR SIDE IMAGING

Just a little over 4 years after the launch of SOHO, Lindsey and Brown (2000) published an astonishing result: the first successful, holographic reconstruction of solar farside features from p-mode oscillations observed on the visible hemisphere with MDI. In the meantime, the astonishing has become routine, and the SOHO MDI offers daily farside images on the Web<sup>1</sup>.

---

<sup>1</sup> <http://soi.stanford.edu/data/farside/>

Another method to monitor solar activity on the far side of the Sun was developed by the SWAN team (Bertaux *et al.*, 2000). SWAN monitors the whole sky in Ly- $\alpha$  light from the Sun, as it is reflected off neutral hydrogen seeping into the heliosphere from the outside. Since active regions are brighter than quiet regions, parts of the sky facing an active region are brighter than those facing a quiet region. Just as a rotating lighthouse beam will illuminate different patches of fog, the Sun's rotation produces a changing pattern of illumination on the sky behind the Sun's far side.

### 3.10. SUBSURFACE STRUCTURE OF SUNSPOTS

The high-resolution data from MDI have allowed new investigations about the structure and flows beneath sunspots (Kosovichev *et al.*, 2000, Zhao *et al.*, 2001). Kosovichev *et al.* (2000) found sunspot “fingers” – long, narrow structures at a depth of about 4 Mm, which connect the sunspot with surrounding pores of the same polarity. Pores which have the opposite polarity are not connected to the spot. The work by Zhao *et al.* provided new clues to a longstanding problem in solar physics: Why do sunspots stay organised for several weeks, instead of disintegrating much more rapidly? The answer appears to be sub-surface inflows. Zhao *et al.* detected strong converging and downward directed flows at depths of 1.5–5 Mm, which they tentatively identified with the downdrafts and vortex flows that were suggested by Parker (1979) for a cluster model of sunspots. In deeper layers, 6–9 Mm, the sunspot region is occupied by a ring of upflows with almost zero velocity at the center. Strong outflows extending more than 30 Mm are found below the downward and converging flows. The analysis by Zhao *et al.* also suggests that sunspots might be a relatively shallow phenomenon, with a depth of 5–6 Mm, as defined by its thermal and hydrodynamic properties. They also found a strong mass flow across the sunspot at depths of 9–12 Mm, which they interpret as more evidence in support of the cluster model, as opposed to the monolithic sunspot model.

### 3.11. EMERGING ACTIVE REGIONS

There have been several attempts to detect emerging active regions in the convection zone before they appeared on the surface (e.g. Kosovichev *et al.*, 2000). It was found that the emerging flux propagates very rapidly in the upper 20 Mm, with a speed exceeding 1 km/s. Early detection of emerging active regions, therefore, may prove difficult without probing deeper into the convection zone.

### 3.12. SUPERGRANULATION

By applying the new technique of time-distance helioseismology to high resolution MDI data, Duvall *et al.* (1997) were able to generate the first maps of horizontal and vertical flow velocities as well as sound speed variations in the convection zone just below the visible surface. They found that in the upper layers, 2–3 Mm deep, the horizontal flow is organized in supergranular cells, with outflows from the cell centers. The characteristic size of these cells is 20–30 Mm and the cell boundaries were found to coincide with the areas of enhanced magnetic field. The supergranulation outflow pattern disappears at a depth of approximately 5 Mm. This suggests that supergranules, which have a characteristic horizontal cell size of 20–30 Mm, are a relatively shallow phenomenon.

The importance of supergranular flows for the distribution of solar magnetic flux and the formation of magnetic network is well known. By using long series (up to 9 days) of subsurface flow maps obtained from MDI Dynamics data by time-distance helioseismology, Gizon *et al.* (2003) have studied the global dynamics of the supergranular flow pattern. They concluded that it has a significant, wave-like component that may explain why this pattern rotates faster than magnetic features in the photosphere, and also why advection may be suppressed by meridional flows.

### 3.13. SEISMIC WAVES

MDI has also made the first observations of seismic waves from a solar flare (Kosovichev and Zharkova, 1998), opening up possibilities of studying both flares and the solar interior. During the impulsive phase of the X2.6 class flare of 9 July 1996 a high-energy electron beam heated the chromosphere, resulting in explosive evaporation of chromospheric plasma at supersonic velocities. The upward motion was balanced by a downward recoil in the lower chromosphere which excited propagating waves in the solar interior. On the surface the outgoing circular flare waves resembled ripples from a pebble thrown into a pond. The seismic wave propagated to at least 120,000 km from the flare epicenter with an average speed of about 50 km/s on the solar surface.

### 3.14. SOLAR OBLATENESS

High precision MDI measurements of the Sun's shape and brightness obtained during two special 360° roll maneuvers of the SOHO spacecraft have produced the most precise determination of solar oblateness ever (Kuhn *et al.*, 1998). There is no excess oblateness. These measurements unambigu-

ously rule out the possibility of a rapidly rotating core, and any significant solar cycle variation in the oblateness.

#### 4. Transition Region and Corona

##### 4.1. UV AND EUV SPECTRAL ATLASES

A far-ultraviolet and extreme-ultraviolet spectral atlas of the Sun between 670 Å and 1609 Å, derived from observations obtained with the SUMER spectrograph (Fig. 5), identifies over 1100 distinct emission lines, of which more than 150 had not been recorded or identified before (Curdt *et al.*, 2001). The atlas contains spectra of the average quiet Sun, a coronal hole and an active region on the disk, providing a rich source of new diagnostic tools to study the physical parameters in the chromosphere, the transition region and the corona. In particular, the wavelength range below 1100 Å as observed by SUMER represents a significant improvement over the spectra produced in the past.

Brooks *et al.* (1999) present the extreme-ultraviolet spectrum as observed in normal incidence by CDS. It covers the wavelength ranges 308–381 Å and 513–633 Å. In all over 200 spectral lines have been measured and about 50% identified.

These two atlases will be a very valuable product for many years to come, for both solar and stellar communities.

##### 4.2. EXPLOSIVE EVENTS AND BLINKERS

Explosive events have been studied extensively by a number of authors (e.g. Innes *et al.*, 1997; Chae *et al.*, 1998), who provided strong evidence that these features are the result of magnetic reconnection. Innes *et al.* (1997) report explosive events that show spatially separated blue shifted and red shifted jets and some that show transverse motion of blue and red shifts, as predicted if reconnection was the source. Chae *et al.* (1998) provide further evidence of the magnetic reconnection origin of explosive events by comparing their SUMER observations with MDI magnetograms and magnetograms obtained at Big Bear Solar Observatory. The explosive events are found to rarely occur in the interior of strong magnetic flux concentrations. They are preferentially found in regions with weak and mixed polarity, and the majority of these events occur during “cancellation” of photospheric magnetic flux (Chae *et al.*, 1998).

Harrison *et al.* (1999) present a thorough and comprehensive study of EUV flashes, also known as “blinkers” (Harrison, 1997), which were identified in quiet Sun network as intensity enhancements of order 10–40% using CDS. They have analyzed 97 blinker events and identified blinker

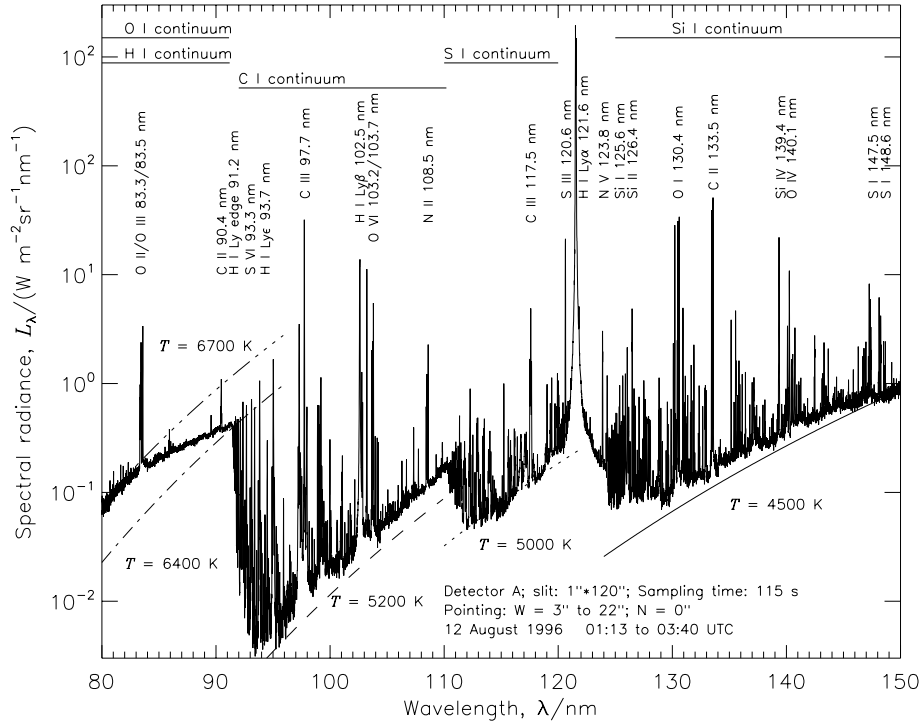


Figure 5. SUMER radiance spectrum of a quiet-Sun region in first order of diffraction (second-order lines have been removed manually). Prominent lines and continua are identified. Some black-body radiation levels are shown to provide an estimate of the radiation temperatures of the continua. From Wilhelm *et al.*, 2002.

spectral, temporal and spatial characteristics, their distribution, frequency and general properties, across a broad range of temperatures, from 20,000 K to 1,200,000 K. The blinkers are most pronounced in the transition region lines O III, O IV and O V, with modest or no detectable signature at higher and lower temperatures. A typical blinker has a duration of about 1000 s. Due to a long tail of longer duration events, the average duration is 2400 s, though. Comparison to plasma cooling times led to the conclusion that there must be continuous energy input throughout the blinker event. The projected blinker onset rate for the entire solar surface is  $1.24 \text{ s}^{-1}$ , i.e. at any one time there are about 3000 blinker events in progress. Remarkably, line ratios from O III, O IV and O V show no significant change throughout the blinker event, suggesting that the intensity increase is not a temperature effect but predominantly caused by increases in density or filling factor. The authors estimate the thermal energy content of an average blinker at  $2 \times 10^{25} \text{ erg}$ .

#### 4.3. ACTIVE REGION DYNAMICS

EIT, SUMER, and CDS observations have clearly demonstrated that the solar transition region and corona is extremely dynamic and time variable in nature. This has become even more evident with the advent of the spectacular high resolution time lapse sequences obtained by the Transition Region and Coronal Explorer (TRACE) (Schrijver *et al.*, 1999). A comprehensive investigation of active region flows by Kjeldseth-Moe and Brekke (1998) demonstrated that high Doppler shifts are common in active region loops. Strong shifts are present in parts of loops for temperatures up to 0.5 MK. Regions with both red and blue shifts are seen. While typical values correspond to velocities of  $\pm 50$ –100 km/s, shifts approaching 200 km/s have been detected. At temperatures  $T \geq 1$  MK, i.e. in Mg ix 368 Å or Fe xvi 360 Å, only small shifts are seen. Thus, the high Doppler shifts seem to be restricted to the chromosphere and transition region.

Fludra *et al.* (1997) show that loops with different temperatures can co-exist within an active region, sometimes very close to each other, but not really co-spatial, i.e. they occupy different volumes.

#### 4.4. CORONAL HOLE TEMPERATURES

Using the two SOHO spectrometers CDS and SUMER, David *et al.* (1998) have measured the electron temperature as a function of height above the limb in a polar coronal hole. Temperatures of around 0.8 MK were found close to the limb, rising to a maximum of less than 1 MK at  $1.15 R_{\odot}$ , then falling to around 0.4 MK at  $1.3 R_{\odot}$ . In equatorial streamers, on the other hand, the temperature was found to rise constantly with increasing distance, from about 1 MK close to the limb to over 3 MK at  $1.3 R_{\odot}$ . With these low temperatures, the classical Parker mechanism cannot alone explain the high wind velocities, which must therefore be due to the direct transfer of momentum from MHD waves to the ambient plasma.

Wilhelm *et al.* (1998) determined the electron temperatures, densities and ion velocities in plumes and interplume regions of polar coronal holes from SUMER spectroscopic observations of the Mg ix 706/750 Å and Si viii 1440/1445 Å line pairs. They find the electron temperature  $T_e$  to be less than 800,000 K in a plume in the range from  $r = 1.03$  to  $1.60 R_{\odot}$ , decreasing with height to about 330,000 K. In the interplume lanes, the electron temperature is also low, but stays between 750,000 and 880,000 K in the same height interval. Doppler widths of O vi lines are narrower in the plumes ( $v_{1/e} \approx 43$  km/s) than in the interplumes ( $v_{1/e} \approx 55$  km/s). Thermal and turbulent ion speeds of Si viii reach values up to 80 km/s, corresponding to a kinetic ion temperature of  $10^7$  K.

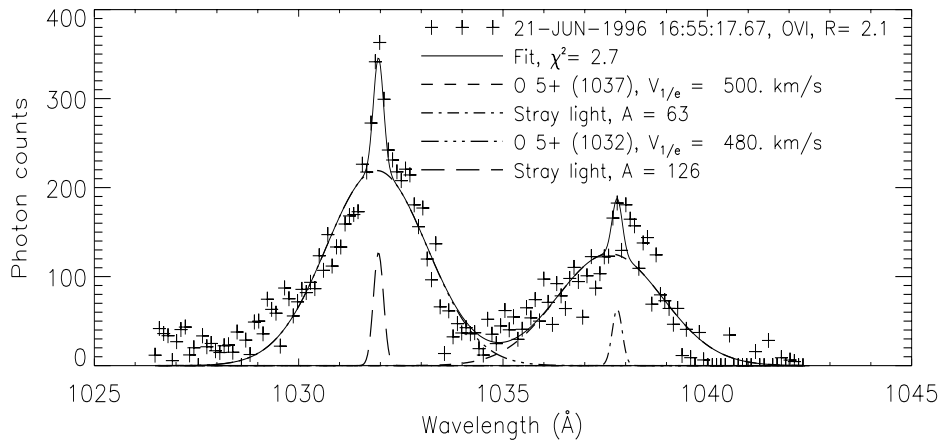


Figure 6. UVCS observations of O VI 1032 Å and 1037 Å above the north polar coronal hole at  $2.1 R_{\odot}$ . The narrow peaks are due to straylight. The data points are shown as crosses, fitted profile by a solid line. (From Kohl *et al.*, 1997.)

One of the most surprising results from SOHO has been the extremely broad coronal profiles of highly ionized elements such as oxygen and magnesium (Kohl *et al.*, 1997, 1999; Fig. 6). Kohl *et al.* (1998) and Cranmer *et al.* (1999a) present a self-consistent empirical model of a polar coronal hole near solar minimum, based on H I and O VI UVCS spectroscopic observations. Their model describes the radial and latitudinal distribution of the density of electrons, H I and O VI as well as the outflow velocity and unresolved anisotropic most probable velocities for H I and O VI. It provides strong evidence of anisotropic velocity distributions for protons and O VI in polar coronal holes (Fig. 7) and indicates proton outflow speeds of  $190 \pm 50$  km/s and larger outflow speeds of  $350 \pm 100$  km/s for O VI at  $2.5 R_{\odot}$ . While the protons (which are closely coupled to H I atoms by charge transfer in the inner corona) are only mildly anisotropic above  $2-3 R_{\odot}$  and never exceed 3 MK, the O VI ions are strongly anisotropic at these heights, with perpendicular kinetic temperatures approaching 200 MK at  $3 R_{\odot}$  and  $(T_{\perp}/T_{\parallel}) \approx 10-100$  (Kohl *et al.*, 1997, 1998). The measured O VI and Mg x “temperatures” are neither mass proportional nor mass-to-charge proportional when compared to H I (Esser *et al.*, 1999; Zangrilli *et al.*, 1999). This and the highly anisotropic velocity distributions rule out thermal (common temperature) Doppler motions and bulk transverse wave motions along the line of sight as dominant line-broadening mechanisms. Clearly, additional energy deposition is required which preferentially broadens the perpendicular velocity of the heavier ions (cf. Section 4.8).

In summary, SOHO measurements have clearly established that the

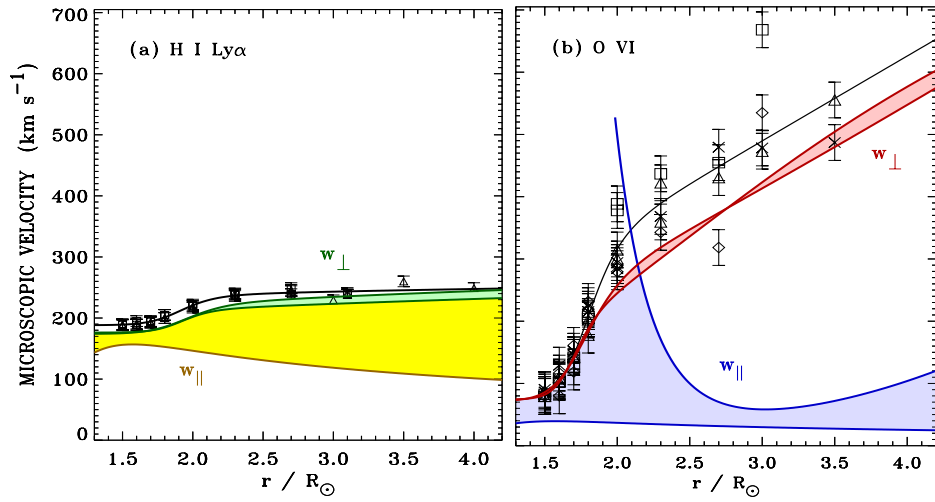


Figure 7.  $v_{1/e}$  and most probable speeds for H I Ly $\alpha$  (left) and O VI 1032 Å (right). Squares: north polar holes, triangles: south polar holes. Solid line: best fit to data. Dotted line: most probable speed  $w_e$  corresponding to the electron temperature. (From Kohl *et al.*, 1998.)

ions in coronal holes are extremely “hot” and the electrons much “cooler”. They also clearly demonstrate that local thermal equilibrium does not exist in polar coronal holes and that the assumption of Collisional Ionization Equilibrium (CIE) and the common notion that  $T_e \approx T_{ion}$  can no longer be made in models of coronal holes.

It seems difficult to reconcile these low electron temperatures measured in coronal holes with the freezing-in temperatures deduced from ionic charge composition data (e.g. Geiss *et al.*, 1995). The freezing-in concept, however, assumes that the adjacent charge states are in ionization equilibrium. A critical re-evaluation of this concept appears to be justified.

#### 4.5. CORONAL HEATING

A promising theoretical explanation for the high temperatures of heavy ions and their strong velocity anisotropies is the efficient dissipation of high-frequency waves that are resonant with ion-cyclotron Larmor motions about the coronal magnetic field lines. This effect has been studied in detail by Cranmer *et al.* (1999b), who constructed theoretical models of the nonequilibrium plasma state of the polar solar corona using empirical ion velocity distributions derived from UVCS and SUMER. They found that the dissipation of relatively small amplitude high-frequency Alfvén waves (10–10,000 Hz) via gyroresonance with ion cyclotron Larmor motions can explain many of the kinetic properties of the plasma, in particular the strong



anisotropies, the greater than mass proportional temperatures, and the faster outflow of heavy ions in the high speed solar wind. Because different ions have different resonant frequencies, they receive different amounts of heating and acceleration as a function of radius, exactly what is required to understand the different features of the H I and O VI velocity distributions. Further, because the ion cyclotron wave dissipation is rapid, the extended heating seems to demand a constantly replenished population of waves over several solar radii. This suggests that the waves are generated gradually throughout the wind rather than propagate up from the base of the corona.

In addition to measuring velocity and intensity oscillation, MDI also measures the line-of-sight component of the photospheric magnetic field. In long, uninterrupted MDI magnetogram series a continuous flux emergence of small bipolar regions has been observed (Schrijver *et al.*, 1997, 1998). Small magnetic bipolar flux elements are continually emerging at seemingly random locations. These elements are rapidly swept by granular and mesogranular flows to supergranular cell boundaries where they cancel and replace existing flux. The rate of flux generation of this “magnetic carpet” is such that all of the flux is replaced in about 40 hours (Schrijver *et al.*, 1998), with profound implications for coronal heating on the top side and questions of local field generation on the lower side of the photosphere. Estimates of the energy supplied to the corona by “braiding” of large-scale coronal field through small-scale flux replacement indicate that it is much larger than that associated with granular braiding (Schrijver *et al.*, 1998).

#### 4.6. POLAR PLUMES

Previously, plumes were considered to be the source regions of the high speed solar wind. Given the narrower line widths in plumes and the absence of any significant motions in plumes, Wilhelm *et al.* (1998) suggested that the source regions of the fast solar wind are the interplume lanes rather than the plumes, since conditions there are far more suitable for a strong acceleration than those prevailing in plumes. Teriaca *et al.* (2003), by applying the Doppler dimming technique to SUMER and UVCS O VI and H I data, present further evidence that is indeed the interplume areas that are the source regions of the fast wind stream. Contrary to that and other published results (e.g. Giordano *et al.*, 2000), Gabriel *et al.* (2003), by applying the Doppler dimming technique to SUMER observations of plumes in the height range of  $1.05 - 1.35 R_{\odot}$ , find that outflow velocities in plumes *exceed* those in the interplume regions. Clearly, the question about the physical nature of plumes and interplumes and their respective role for the acceleration of the fast wind streams is still far from settled.

DeForest and Gurman (1998) observed quasi-periodic compressive waves in solar polar plumes in EIT Fe IX/X 171 Å time sequences. The pertur-

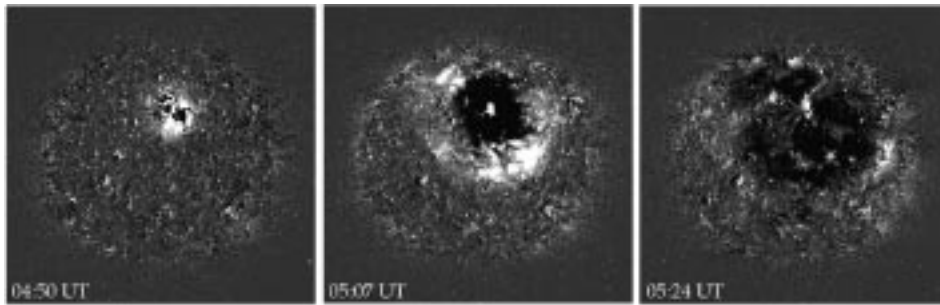


Figure 8. SOHO/EIT 195 Å running difference images of the EIT-wave event of 12 May 1997. The brightest regions exceed 200 percent increase in emission measure. From Thompson *et al.*, 1998.

bations amount to 10–20% of the plumes’ overall intensity and propagate outward at 75–150 km/s, taking the form of wave trains with periods of 10–15 minutes and envelopes of several cycles. The authors conclude that the perturbations are compressive waves (such as sound waves or slow-mode acoustic waves) propagating along the plumes. Assuming that the waves are sonic yields a mechanical flux of  $1.5\text{--}4 \times 10^5 \text{ ergs cm}^{-2} \text{ s}^{-1}$  in the plumes. The energy flux required to heat a coronal hole is about  $10^6 \text{ ergs cm}^{-2} \text{ s}^{-1}$ .

#### 4.7. EIT WAVES

EIT has discovered large-scale transient waves in the corona, sometimes also called “Coronal Moreton Waves”, propagating outward from active regions below CMEs (Thompson *et al.*, 1998, 1999). These events are usually recorded in the Fe XII 195 Å bandpass, during high-cadence ( $\leq 20$  min) observations. Their appearance is stunning in that they usually affect most of the visible solar disk (Fig. 8). They generally propagate at speeds of 200–500 km/s, traversing a solar diameter in less than an hour. Active regions distort the waves locally, bending them toward the lower Alfvén speed regions. On the basis of speed and propagation characteristics, Thompson *et al.* (1998, 1999) associate the “EIT waves” with fast-mode MHD waves. Another interesting aspect of these waves is their association with the acceleration and injection of high energy electrons and protons (Torsti *et al.*, 1999).

#### 4.8. HOT LOOP OSCILLATIONS

Kliem *et al.* (2002) have discovered strong Doppler shift oscillations in SUMER observations of hot loops above active regions (Fig. 9). Wang *et al.* (2003) give an extensive overview of hot coronal loop oscillations and identify them with slow magnetoacoustic standing waves in the loops. The

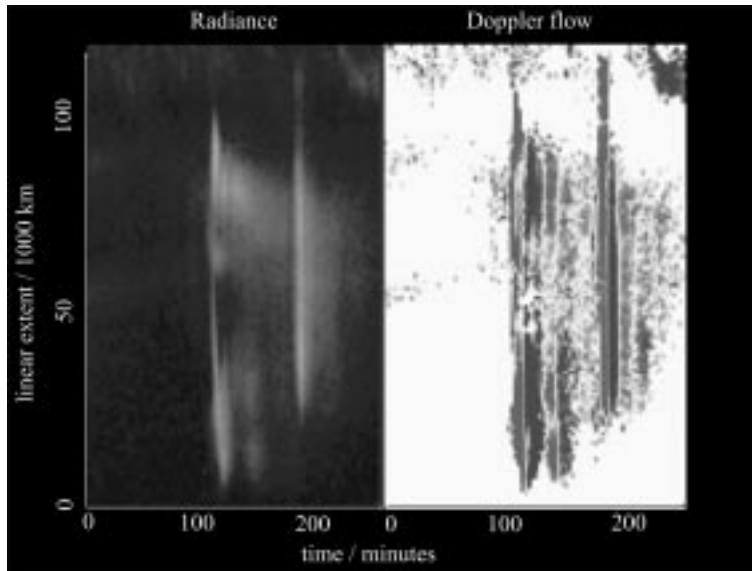


Figure 9. Hot loop oscillations as observed by SUMER in Fe XIX 1118 Å. Left: intensity; right: velocity. Time goes from left to right in each half. Courtesy W. Curdt/SUMER.

periods are typically around 10 to 20 minutes, with a comparable decay time scale. The oscillations are seen only in hot flare lines ( $>6$  MK, e.g. Fe XVII, Fe XIX, Fe XXI). Lines formed at “normal” coronal temperatures (1 MK, e.g. Fe XII, Ca XIII, Ca X) do not show any signature of these oscillations. These new and previously unexpected results may help to understand the heating of coronal loops, and open a new area of coronal seismology.

## 5. Solar Wind

### 5.1. ORIGIN AND ACCELERATION OF THE FAST SOLAR WIND

Coronal hole outflow velocity maps obtained with the SUMER instrument in the Ne VIII emission line at 770 Å show a clear relationship between coronal hole outflow velocity and the chromospheric network structure, with the largest outflow velocities occurring along network boundaries and at the intersection of network boundaries (Hassler *et al.*, 1999). This can be considered the first direct spectroscopic determination of the source regions of the fast solar wind in coronal holes.

Proton and  $O^{5+}$  outflow velocities in coronal holes have been measured by UVCS using the Doppler dimming method (Kohl *et al.*, 1997, 1998; Cranmer *et al.*, 1999a). The  $O^{5+}$  outflow velocity was found to be significantly higher than the proton velocity, with a very steep increase between 1.5 and 2.5  $R_{\odot}$ , reaching outflow velocities of 300 km/s already around

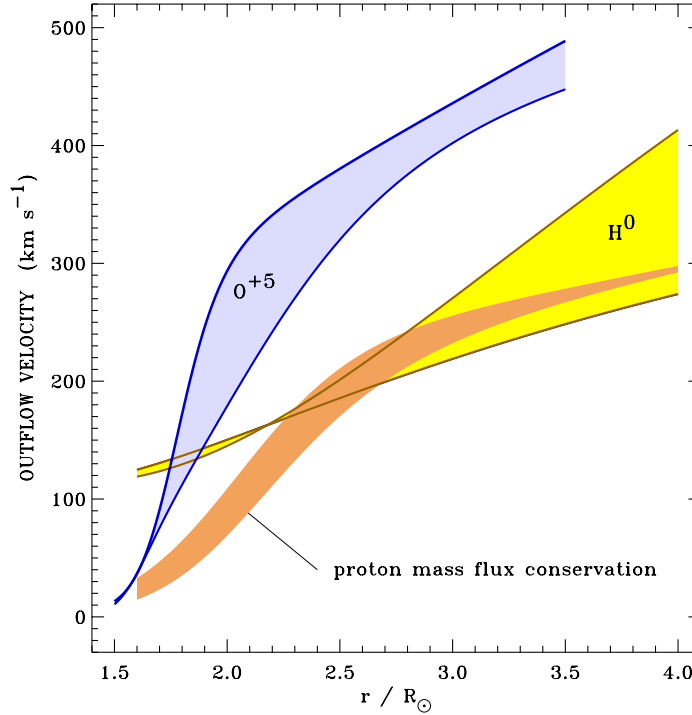


Figure 10. Empirical outflow velocity of O VI and H I in polar coronal holes, with gray regions corresponding to lower/upper limits of  $w_{||}$ . From Kohl *et al.*, 1998.

$2 R_{\odot}$  (Fig. 10). While the hydrogen outflow velocities are still consistent with some conventional theoretical models for polar wind acceleration, the higher oxygen flow speeds cannot be explained by these models. A possible explanation is offered by the dissipation of high-frequency Alfvén waves via gyroresonance with ion-cyclotron Larmor motions, which can heat and accelerate ions differently depending on their charge and mass (Cranmer *et al.*, 1999b, and references therein).

## 5.2. ACCELERATION, ORIGIN AND COMPOSITION OF THE SLOW SOLAR WIND

Time-lapse sequences of LASCO white-light coronagraph images give the impression of a continuous outflow of material in the streamer belt. Density enhancements, or “blobs” form near the cusps of helmet streamers and appear to be carried outward by the ambient solar wind. Sheeley *et al.* (1997), using data from the LASCO C2 and C3 coronagraphs, have traced a large number of such “blobs” from 2 to over 25 solar radii. Assuming that

these “blobs” are carried away by the solar wind like leaves on the river, they have measured the acceleration profile of the slow solar wind, which typically doubles from 150 km/s near  $5 R_{\odot}$  to 300 km/s near  $25 R_{\odot}$ . They found a constant acceleration of about  $4 \text{ m s}^{-2}$  through most of the  $30 R_{\odot}$  field-of-view. The speed profile is consistent with an isothermal solar wind expansion at a temperature of about 1.1 MK and a sonic point near  $5 R_{\odot}$ .

Raymond *et al.* (1997) analyzed UVCS data to measure the composition of coronal streamers. They found strong variations from streamer to streamer, and even within streamers. The FIP effect is present in streamers, and the helium abundance lower than in the photosphere. In the core of quiescent equatorial streamers, oxygen and other high-FIP elements are depleted by an order of magnitude compared to photospheric abundances, while they are depleted by only a factor of 3 along the edges of the streamers. They suggest that gravitational settling may be responsible for the low abundances of heavy elements in the static core region of closed magnetic field. The abundance along the edges of the streamer (“legs”) resemble elemental abundances measured in the slow solar wind, suggesting the identification of streamers as the source regions of that wind component.

Uzzo *et al.* (2003) combined UVCS and CELIAS measurements to determine abundances of oxygen, silicon, and magnesium in streamers and the slow solar wind on an almost daily basis over more than 2 months during solar minimum conditions (summer of 1996). The agreement between remote sensing and *in-situ* measurements provides further evidence that active-region streamers and the outer “leg” structural component of quiescent streamers are contributors to the slow solar wind.

Kallenbach *et al.* (1997), using CELIAS/MTOF data, has made the first *in-situ* determination of the solar wind calcium isotopic composition, which is important for studies of stellar modelling and solar system formation, because the present-day solar Ca isotopic abundances are unchanged from their original isotopic composition in the solar nebula. The isotopic ratios  $^{40}\text{Ca}/^{42}\text{Ca}$  and  $^{40}\text{Ca}/^{44}\text{Ca}$  measured in the solar wind are consistent with terrestrial values.

The first in-situ determination of the isotopic composition of nitrogen in the solar wind has been made by Kallenbach *et al.* (1998), also based on CELIAS/MTOF data. They found an isotope ratio  $^{14}\text{N}/^{15}\text{N} = 200 \pm 60$ , indicating a depletion of  $^{15}\text{N}$  in the terrestrial atmosphere compared to solar matter.

Ipavich *et al.* (2001) report relative abundances of the iron isotopes  $^{54}\text{Fe}$ ,  $^{56}\text{Fe}$ , and  $^{57}\text{Fe}$ . Their results agree with terrestrial values. Bochsler *et al.* (2000) have measured the abundance of aluminum in the solar wind. The Al/Mg abundance ratio is important because it provides an excellent test case for investigating possible fractionation processes among low FIP

elements in the solar wind. In interstream solar wind regimes they measured a ratio of  $0.081 \pm 0.012$ , and in a coronal hole associated high speed wind stream  $0.076 \pm 0.011$ . A comparison with the solar system ratio of  $0.079 \pm 0.005$  gives no indication of fractionation occurring among low FIP elements in the solar wind.

## 6. CMEs and Space Weather

The LASCO team has compiled an extensive list<sup>2</sup> and catalog<sup>3</sup> (Yashiro *et al.*, 2004) of the more than 6000 coronal mass ejections observed with SOHO since launch. The on-line catalog of Yashiro *et al.* (2004) documents the observed properties of all CMEs observed by LASCO, such as central position angle, angular width in the plane of sky, heliocentric distance with time, average speed, and acceleration.

St.Cyr *et al.* (2000) report the properties of all the 841 CMEs observed by the LASCO C2 and C3 white-light coronagraphs from January 1996 through the SOHO mission interruption in June 1998 and compare those properties to previous observations by other instruments. The CME rate for solar minimum conditions was slightly higher than had been reported for previous solar cycles, but both the rate and the distribution of apparent locations of CMEs varied during this period as expected. The general shape of the distribution of apparent sizes for LASCO CMEs is similar to those of earlier reports, but the average (median) apparent size of  $72^\circ$  ( $50^\circ$ ) is significantly larger.

St.Cyr *et al.* (2000) also report on a population of CMEs with large apparent sizes, which appear to have a significant longitudinal component directed along the Sun-Earth line, either toward or away from the Earth (so-called “halo” CMEs). Using full disk EIT images they found that 40 out of 92 of these events might have been directed toward the Earth. A comparison of the timing of those events with the Kp geomagnetic storm index in the days following the CME yielded that 15 out of 21 (71%) of the Kp > 6 storms could be accounted for as SOHO LASCO/EIT frontside halo CMEs. Eliminating three Kp storms that occurred following LASCO/EIT data gaps brings the possible association rate to 18 out of 21 (86%).

Fox *et al.* (1998) describe the first ever end to end tracking of a space storm (6–10 January 1997 event), from its eruption on the Sun to its impact at Earth.

Gopalswamy *et al.* (2003) studied the solar cycle variations of various properties of CMEs, such as daily CME rate, mean and median speeds, and the latitude of solar sources for cycle 23 (1996-2002). They find that (1)

---

<sup>2</sup> <http://lasco-www.nrl.navy.mil/cmelist.html>

<sup>3</sup> [http://cdaw.gsfc.nasa.gov/CME\\_list/](http://cdaw.gsfc.nasa.gov/CME_list/)

there is an order of magnitude increase in CME rate from the solar minimum (0.5/day) to maximum (6/day), (2) the maximum rate is significantly higher than previous estimates, (3) the mean and median speeds of CMEs also increase from minimum to maximum by a factor of 2, (3) the latitude distribution of CMEs separate the prominence-associated (high-latitude) and active-region associated CMEs, and (4) the rate of high-latitude CMEs shows north-south asymmetry and the cessation eruptions in the north and south roughly mark the polarity reversals. They also compared the rates of the fast-and-wide CMEs, major solar flares, interplanetary shocks, long-wavelength type II bursts and large SEP events and conclude that all these phenomena (except the major flares, which are too frequent) have a close physical relationship.

Simnett *et al.* (2002) compared the release time of near-relativistic electron beams ( $\approx 40\text{--}300\text{ keV}$ ) measured by ACE with the timing of coronal activity measured by LASCO. They found that the near-relativistic electron injection time was typically delayed by approximately 20 minutes from the CME launch time and greater than 10 minutes after the onset of the electromagnetic radio and X-ray signatures of the flare (when present). Therefore, the near-relativistic electrons that must be present to produce the chromospheric electromagnetic emission do not escape promptly (at least in detectable quantities). The radial distance of most CMEs at the electron release time was between 1.5 and 3.5  $R_{\odot}$ . Both the peak electron flux and the spectral hardness of the electrons were positively correlated with the CME speed, a signature of shock acceleration. They therefore suggest that most of the near-relativistic electrons seen by ACE/EPAM are accelerated by the shock driven by the coronal transient and are released at a radial distance around 2–3  $R_{\odot}$ .

Torsti *et al.* (2002) present the first ever measurement of the  $^3\text{He}$  energy spectrum of an event with an exceptionally high  $^3\text{He}$  enhancement ( $^3\text{He}/^4\text{He} > 1$ ). The particle event was associated with an impulsive flare and an interplanetary shock wave. The analysis shows that the high-energy  $^3\text{He}$ -rich event refers to the flare material reaccelerated by the interplanetary CME. Onset of the high-energy  $^3\text{He}$ -rich event was observed in the far upstream region, when the CME-driven shock was at about 0.3 AU from the Sun.

## 7. Heliosphere

The Sun is moving through the Local Interstellar Cloud (LIC) at a velocity of about 26 km/s. The solar wind builds a cavity, the heliosphere, within the ionized gas component of the LIC. The neutral gas component at of the LIC however passes through the heliopause and into the heliosphere,

where it can be observed by SWAN. Costa *et al.* (1999) analysed SWAN H-cell data and compared them with a simple hot model of the interstellar H flow in the inner heliosphere. They found hydrogen temperatures  $T_0$  of  $11,500 \pm 1500$  K, i.e. significantly above the temperature of the interstellar He flow ( $6000 \pm 1000$  K), requiring a strong heating of more than 3500 K at the heliosphere interface. Part of this excess temperature probably is due to radiative transfer effects. They also measured a deceleration of the interstellar hydrogen at the heliopause of  $3.5 \pm 1.0$  km/s.

Quémerais *et al.* (1999), in an independent study using data from the SWAN hydrogen absorption cell, determined the apparent interstellar hydrogen velocity in the up- and downwind direction to  $-25.4 \pm 1$  km/s and  $+21.6 \pm 1.3$  km/s, respectively. They also presented the most precise, model independent determination of the H flow direction. Their new estimate of the upwind direction is  $252.3^\circ \pm 0.73^\circ$  and  $8.7^\circ \pm 0.90^\circ$  in ecliptic coordinates, which is off by about  $3^\circ$ – $4^\circ$  from the He flow direction. The authors speculate that this might be a sign of an asymmetry of the heliospheric interface due to the ambient interstellar magnetic field.

Comparing the above hydrogen temperature and velocity measurements by SWAN with heliospheric models leads to an estimate of the interstellar plasma density of  $n_e \approx 0.04 \text{ cm}^{-3}$  (Lallement, 1999). It is interesting to note that the plasma frequency for  $n_e = 0.04 \text{ cm}^{-3}$  is 1.8 kHz, i.e. exactly the value of the remarkably stable cut-off frequency observed by Voyager.

## 8. Comets

SOHO is providing new measurements not only about the Sun. As of the end of 2003 LASCO has detected over 700 comets, most of them so-called sun-grazers. One comet was discovered by SWAN in Ly- $\alpha$  emission (Mäkinen *et al.*, 2000).

Biesecker *et al.* (2002) used LASCO observations of comets to obtain quantitative light curves of sungrazing comets. The light curves reveal an anomalous brightening as the comets approach the Sun, followed by a rapid dimming when the comets pass beyond  $\approx 11 R_\odot$ , suggesting break-up around this distance.

Thanks to rapid communication from the LASCO group and the near-realtime observing capabilities of the SOHO instruments due to the unique operations concept, UVCS could make spectroscopy measurements of several comets on the day of their discovery. UVCS spectroscopic measurements of comet C/1996Y1 obtained at  $6.8 R_\odot$  confirmed the predictions of models of the cometary bow shock driven by mass-loading as cometary molecules are ionized and swept up in the solar wind. From the width and shift of the line profiles, the solar wind speed at  $6.8 R_\odot$  could be determined



(640 km/s). The outgassing rate of the comet was estimated at 20 kg/s, implying an active area of the nucleus of only about 6.7 m in diameter and a mass of about 120,000 kg (Raymond *et al.*, 1998).

Uzzo *et al.* (2001) report UVCS Ly- $\alpha$  observations of comet C/ 2000 C6, a member of the Kreutz family of sungrazing comets, which was in the UVCS field-of-view on 9 and 10 February 2000. A tail nearly  $0.5 R_{\odot}$  in length was detected in Ly- $\alpha$  emission. From the Ly- $\alpha$  intensity and its rate of fading due to H I ionization they estimated the streamer density at  $4.56 R_{\odot}$  to  $0.68 \times 10^5 \text{ cm}^{-3}$ . They also determined the outgassing rate at various heights, which in turn gives an estimate of the diameter of the nucleus (12 m). Further, between  $5.7$  and  $4.6 R_{\odot}$  a sudden brightening was observed, which is interpreted as fragmentation of the nucleus.

Mäkinen *et al.* (2001) used the SWAN instrument to monitor the break-up of comet C/1999 S4 (LINEAR). The total amount of water vapour observed by SWAN from 25 May through 12 August 2000 was estimated at  $3.3 \times 10^9 \text{ kg}$ . Only about 1% of this was left on 6 August, when observations by the Hubble Space Telescope of the dying comet's fragments gave an estimate of the total volume of the fragments. Combining the two numbers gives a remarkably low value for the density - about  $15 \text{ kg/m}^3$ , compared with  $917 \text{ kg/m}^3$  for familiar non-porous ice. Even allowing for an equal amount of dust grains,  $30 \text{ kg/m}^3$  is far less than the  $500 \text{ kg/m}^3$  often assumed by cometary scientists.

Combi *et al.* (2000) observed the structure and evolution of the hydrogen Ly- $\alpha$  coma of comet Hale-Bopp (1995 O1) during its perihelion passage in the spring of 1997. The coma was more than 100 million kilometers wide, far exceeding the great comet's visible tail. Although generated by a comet nucleus perhaps only 40 km in diameter, the hydrogen cloud was 70 times wider than the Sun itself and ten times wider than the hydrogen cloud of Comet Hyakutake observed by SWAN in 1996. The water evaporation rate of Hale-Bopp was measured at more than 200 million tons per day. For comparison, comet Wirtanen, the original target of ESA's Rosetta mission, pumped out water vapour at a rate of 20,000 tons per day during its most recent visit to the Sun, according to SWAN data. The SWAN observations of Hale-Bopp have also shown something else extraordinary — the biggest feature ever observed in our solar system, namely the shadow of comet Hale-Bopp's coma projected on the sky behind it.

The analysis of high-resolution spectroscopic observations of comet C/ 2002 X5 (Kudo-Fujikawa) from UVCS has revealed a quasi-spherical cloud of neutral hydrogen and a variable tail of ionized carbon ( $\text{C}^+$  and  $\text{C}^{2+}$ ) that disconnected from the comet and subsequently regenerated (Povich *et al.*, 2003).  $\text{C}^{2+}$  has never been observed in a comet before. The high abundance of  $\text{C}^{2+}$  and  $\text{C}^+$  relative to water (24%) found is unexplainable

by photodissociation of carbon monoxide but instead attributed to the evaporation and subsequent photoionization of atomic carbon from organic refractory compounds present in the cometary dust grains.

Because Venus has no appreciable magnetic field, the solar wind interacts directly with the planetary atmosphere and ionosphere much as with a cometary coma. In fact, several people have pointed out similarities of the tails of Venus and comets. In June 1996, Venus passed through a very close inferior conjunction with the Sun. Close to that time the CELIAS/CTOF sensor registered three intervals of unusual fluxes of  $O^+$  and  $C^+$  (Grünwaldt *et al.*, 1997). The  $C^+$  abundance was  $\approx 10\%$  of  $O^+$ . The energy distributions resembled those of tail rays originating in the Venus ionosphere or ionopause region, i.e. Venus tail rays have been identified in the solar wind some 45 million km downstream of Venus.

## Acknowledgements

The great success of the SOHO mission is a tribute to the many people — too many to name here — who designed and built the SOHO spacecraft and instruments, and to the many people who diligently work behind the scenes to keep it up and running. SOHO is a project of international cooperation between ESA and NASA.

## References

- Ahmad, Q.R., Allen, R.C., Andersen, T.C., *et al.*: 2002, *Phys. Rev. Let.* **89**, 011301  
 Appourchaux, T., Froehlich, C., Andersen, B., *et al.*: 2000, *ApJ* **538**, 401  
 Bahcall, J.N., Ostriker, J.P.: 1997, *Unsolved Problems in Astrophysics*, Princeton Univ. Press  
 Beck, J.G., Gizon, L., Duvall, T.L., Jr.: 2002, *ApJ* **575**, L47  
 Bertaux, J.-L., Quémerais, E., Lallement, R., *et al.*: 2000, *GRL* **27**, 1331  
 Biesecker, D.A., Lamy, P., St.Cyr, O.C., *et al.*: 2002, *Icarus* **157**, 323  
 Bochsler, P., Ipavich, F.M., Paquette, J.A., *et al.*: 2000, *JGR* **105**, No. A6, 12659  
 Brooks, D.H., Fischbacher, G.A., Fludra, A., *et al.*: 1999, *A&A* **347**, 277  
 Chae, J., Wang, H., Lee, C.-Y., Goode, P.R., and Schühle, U.: 1998, *ApJ* **497**, L109.  
 Combi, M.R., Reinard, A.A., Bertaux, J.-L., *et al.*: 2000, *Icarus* **144**, 191  
 Costa, J., Lallement, R., Quémerais, E., *et al.*: 1999, *A&A* **349**, 660  
 Couvidat, S., García, R.A., Turck-Chièze, S., *et al.*: 2003, *ApJ* **597**, L77  
 Cranmer, S.R., Kohl, J.L., Noci, G., *et al.*: 1999a, *ApJ* **511**, 481.  
 Cranmer, S.R., Field, G.B., and Kohl, J.L.: 1999b, *ApJ* **518**, 937.  
 Curdt, W., Brekke, P., Feldman, U., *et al.*: 2001, *A&A* **375**, 591  
 David, C., Gabriel, A.H., Bely-Dubau, F., *et al.*: 1998, *A&A* **336**, L90.  
 DeForest, C.E., Gurman, J.B.: 1998, *ApJ* **501**, L217.  
 Domingo, V., Fleck, B., and Poland, A.I.: 1995, *Solar Phys.* **162**, 1.  
 Duvall, T.L., Jr.: 1979, *Solar Phys.* **63**, 3.  
 Duvall, T.L., Jr., Kosovichev, A.G., Scherrer, P.H., *et al.*: 1997, *Solar Phys.* **170**, 63

- Esser, R., Fineschi, S., Dobrzycka, D., *et al.*: 1999, *ApJ* **510**, L63.
- Fleck, B., Domingo, V., and Poland, A.I. (eds.): 1995, The SOHO Mission, *Solar Phys.* **162**, Nos. 1–2.
- Fludra, A., Brekke, P., Harrison, R.A., *et al.*: 1997, *Solar Phys.* **175**, 487
- Fox, N.J., Peredo, M., Thompson, B.J.: 1998, *GRL*, **Vol. 25, No. 14**, 2461
- Fröhlich, C.: 2003, *Metrologia* **40**, 60
- Fröhlich, C., Lean, J.: 2002, *Astron. Nachr.* **323**, 203
- Gabriel, A.H., Baudin, F., Boumier, P., *et al.*: 2002, *A&A* **390**, 1119
- Gabriel, A.H., Bely-Dubau, F., Lemaire, P.: 2003, *ApJ* **589**, 623
- Geiss, J., Gloeckler, G., von Steiger, R., *et al.*: 1995, *Science* **268**, 1033.
- Giles, P.M., Duvall, T.L., Jr., and Scherrer, P.H.: 1997, *Nature* **390**, 52.
- Giordano, S., Antonucci, E., Noci, G., Romoli, M., Kohl, J.L.: 2000, *ApJ* **531**, L79
- Gizon, L., Duvall, T.L., Jr., Schou, J.: 2003, *Nature* **421**, 43
- Gopalswamy, N. Lara, A., Yashiro, S., Nunes, S., Howard, R.A.: 2003, ESA SP-535, 403
- Grünwaldt, H., Neugebauer, M., Hilchenbach, M., *et al.*: 1997, *GRL* **24**, No.10, 1163
- Haber, D.A., Hindman, B.W., Toomre, J., *et al.*: 2002, *ApJ* **570**, 855
- Hassler, D.M., Dammasch, I., Lemaire, P., *et al.*: 1999, *Science* **283**, 810.
- Harrison, R.A.: 1997, *Solar Phys.* **175**, 467.
- Harrison, R.A., Lang, J., Brooks, D.H., and Innes, D.E.: 1999, *A&A* **351**, 1115.
- Howe, R., Christensen-Dalsgaard, J., Hill, F., *et al.*: 2000a, *ApJ* **533**, L163
- Howe, R., Christensen-Dalsgaard, J., Hill, F., *et al.*: 2000b, *Science* **287**, 2456
- Howe, R.: 2003, ESA SP-517, p. 81
- Innes, D.E., Inhester, B., Axford, W.I., and Wilhelm, K.: 1997, *Nature* **386**, 811.
- Ipavich, F.M., Paquette, J.A., Bochsler, P., Lasley, S.E., Wurz, P.: 2001, in “Solar and Galactic Composition”, ed. R.F. Wimmer-Schweingruber, CP598, p.121
- Kallenbach, R., Ipavich, F.M., Bochsler, P., *et al.*: 1997, *ApJ* **498**, L75.
- Kallenbach, R., Geiss, J., Ipavich, F.M., *et al.*: 1998, *ApJ* **507**, L185.
- Kjeldseth-Moe, O., Brekke, P.: 1998, *Solar Phys.* **182**, 73.
- Kliem, B., Dammasch, I.E., Curdt, W., Wilhelm, K.: 2002, *ApJ* **568**, L61
- Kohl, J.-L., Noci, G., and Antonucci, E., *et al.*: 1997, *Solar Phys.* **175**, 613.
- Kohl, J.-L., Noci, G., Antonucci, E., *et al.*: 1998, *ApJ* **501**, L127.
- Kohl, J.-L., Esser, R., and Cranmer, S.R., *et al.*: 1999, *ApJ* **510**, L59.
- Kosovichev, A.G., Duvall, T.L., and Scherrer, P.H.: 2000, *Solar Phys.*, **192**, 159
- Kosovichev, A.G., Schou, J.: 1997, *ApJ* **482**, L207.
- Kosovichev, A.G., Zharkova, V.V.: 1998, *Nature* **393**, 317.
- Krivova, N.A., Solanki, S.K., Fligge, M., Unruh, Y.C.: 2003, *A&A* **399**, L1
- Kuhn, J.R., Bush, R.I., Scheick, X., Scherrer, P.H.: 1998, *Nature* **392**, 155
- Lallement, R.: 1999, in *Proc. Solar Wind 9*, S. Habbal (ed.), AIP Conf. Proc. 471, 205
- Lindsey, C., Braun, D.C.: 2000, *Science* **287**, 1799
- Mäkinen, T., Bertaux, J.-L., Combi, M.R., Quemerais, E.: 2001, *Science* **292**, 1326
- Mäkinen, T., Bertaux, J.-L., Laakso, H., *et al.*: 2000, *Nature* **405**, 321
- Parker, E.N.: 1979, *ApJ* **230**, 905
- Povich, M.S., Raymond, J.C., Jones, G.H., *et al.*: 2003, *Science* **302**, No. 5652, 1949
- Quémerais, E., Bertaux, J.-L., Lallement, R., and Berthé, M.: 1999, *JGR* **104**, 12 585.
- Raymond, J.C., Fineschi, S., Smith, P.L., *et al.*: 1998, *ApJ* **508**, 410.
- Raymond, J.C., Kohl, J.K., Noci, G., *et al.*: 1997, *Solar Phys.* **175**, 645
- Sheeley, N.R. Jr., Wang, Y.-M., Hawley, S.H., *et al.*: 1997, *ApJ* **484**, 472.
- Schou, J., Antia, H.M., Basu, S., *et al.*: 1998, *ApJ* **505**, 390.
- Schrijver, C.J., Title, A.M., Harvey, K.L., *et al.*: 1998, *Nature* **394**, 152.
- Schrijver, C.J., Title, A.M., van Ballegoijen, A., *et al.*: 1997, *ApJ* **487**, 424

- Schrijver, C.J., Title, A.M., Berger, T.E., *et al.*: 1999, *Solar Phys.* **187**, 261.  
 Simnett, G.M., Roelof, E.C., Haggerty, D.K.: 2002, *ApJ* **579**, 854  
 St. Cyr, O.C., Plunkett, S.P., Michels, D.J., *et al.*: 2000, *GRL* **105**, No. A8, 18,169  
 Teriaca, L., Poletto, G., Romoli, M., Biesecker, D.A.: 2003, *ApJ* **588**, 566  
 Thompson, B.J., Gurman, J.B., Neupert, W.M., *et al.*: 1999, *ApJ* **517**, L151.  
 Thompson, B.J., Plunkett, S.P., Gurman, J.B., *et al.*: 1998, *GRL* **25**, 2465  
 Torsti, J., Kocharov, L., Laivola, J., *et al.*: 2002, *ApJ* **573**, L59  
 Torsti, J., Kocharov, L., Teittinen, M., and Thompson, B.J.: 1999, *ApJ* **510**, 460.  
 Turck-Chièze, S., Couvidat, S., Kosovichev, A.G., *et al.*: 2001, *ApJ* **555**, L69  
 Uzzo, M., Ko, Y.-K., Raymond, J.C., Wurz, P., Ipavich, F.M.: 2003, *ApJ* **585**, 1062  
 Uzzo, M., Raymond, J.C., Biesecker, D., *et al.*: 2001, *ApJ* **558**, 403  
 Vorontsov, S.V., Christensen-Dalsgaard, J., Schou, J., *et al.*: 2002, *Science* **296**, 101  
 Wilhelm, K., Marsch, E., Dwivedi, B.N., *et al.*: 1998, *ApJ* **500**, 1023.  
 Wilhelm, K., Schühle, U., Curdt, W., *et al.*: 2002, in “The Radiometric Calibration of SOHO”, eds. A. Pauluhn *et al.*, ISSI SR-002, p. 145  
 Willson, R.C., Mordvinov, A.V.: 2003, *GRL* **30**, 1199  
 Wang, T.J., Solanki, S.K., Curdt, W., *et al.*: 2003, *A&A* **406**, 1105  
 Yashiro, S., Gopalswamy, N., Michalek, G., *et al.*: 2004, *JGR*, submitted  
 Zangrilli, L., Nicolosi, P., Poletto, G., *et al.*: 1999, *A&A* **342**, 592  
 Zhao, J., Kosovichev, A.G., Duvall, T.L., Jr.: 2001, *ApJ* **557**, 384